International Journal of Development Mathematics Vol 1 Issue 1 Page No. 216 - 227

INTERNATIONAL JOURNAL OF DEVELOPMENT MATHEMATICS

ISSN: 3026-8656 (Print) | 3026-8699 (Online)

journal homepage: https://ijdm.org.ng/index.php/Journals

Irreversibility Analysis for Magnetized and Nonlinear Convection Flow of Carreau Fluid Past a Nonlinear Surface with Higher-Order Adherence Factor

Jos U. Abubakar [a], Mojeed T. Akolade [a,b,*], Hafizat O. Momoh [c], Timothy L. Oyekunle [a] and Florence D. Ayegbusi [d]

[a]Department of Mathematics, University of Ilorin, Ilorin, 240003, Kwara, Nigeria.

[b]Department of Computer Science, Lead City University, Ibadan, Nigeria.

[c]Department of Mathematics and Statistics, Federal Polytechnic Nasarawa, Nasarawa, Nigeria.

[d]Department of Mathematics and Statistics First Technical University, Ibadan.

ARTICLE INFO

Article history:
Received 20 December 2023
Received in revised form 20 February 2024
Accepted 07 March 2024

Keywords:
Carreau fluid, Entropy generation Momentum slip, Nonlinear Convection, Pseudo spectral method

MSC 2020 Subject classification:
34A25, 34B15, 34L05, 76A05, 76D05.

ABSTRACT

Studying entropy generation allows scientists and engineers to optimize processes, design more efficient systems, and develop sustainable technologies. These studies aim towards minimizing energy losses, reducing environmental impacts, and advancing the frontiers of thermodynamics and energy science. As such, the current investigation expunges the dynamics of heat, flow, entropy and irreversibility analysis for a magnetized and dissipative Carreau fluid flow over a nonlinearly stretching sheet. The model is subject to thermal and electrical conductivity variations, higher-order adherence factors and nonlinear convective motion over an inclined nonlinear surface. Herein, the heat source in the flow system is considered space and temperature-dependent. The mathematical model presented in PDE systems is transformed to ODEs via similarity transformation. Numerically, the solutions to the distribution profiles are approximated via Chebyshev Collocation Method (CCM) with the pseudospectra (differentiation matrix) technique. In the limited case, the results here benchmark existing literature. Our findings identified that thermal irreversibility dominated the entire flow system, further entropy generation and irreversibility enhancement requires more thermal energy. We as well elucidate that alteration of both heat source modulation affects the heat transfer coefficient while Joule heating effect generates inner energy which induces the Carreau fluid energy.

1. Introduction

Entropy generation, deeply rooted in the second law of thermodynamics, asserts that the total entropy of a closed system tends to increase over time, reaching its maximum at equilibrium (Bejan, 1995; 1996; 2002; Lone *et al*., 2024). Understanding this concept is crucial as it sheds light on the irreversibility of processes and the directionality of natural phenomena. Central to entropy generation is the notion of disorder or randomness within a system (Sciacovelli *et al*., 2015; Zhang *et al*., 2024). Practically, entropy generation imposes constraints on the efficiency of energy conversion processes and the feasibility of technological advancements. It governs the direction of heat flow, engine behavior, refrigeration cycle efficiency, and various other aspects of thermodynamic systems (Akolade, 2023; Rashidi *et al*., 2021; Ogunsola and Oyedotun, 2023). Among investigations into this fundamental concept of thermodynamics is the study of Carreau fluid flow in microchannels by Shehzad *et al*. (2020), Shashikumar *et al*. (2022), and Reedy *et al*. (2022). These studies incorporate second law analysis, thermal radiative heat, and other parameters in nonlinear stretching surfaces. Additionally, Raza *et al*. (2020) modeled flow dynamics on linearly coiled curved stretchable surfaces, examining the impact of curvature parameters through the lens of the entropy generation law, among other significant studies.

The physics of the adherence factor is crucial for various fields, including materials science, surface engineering, and biophysics, as it quantifies the adhesion strength between two materials or surfaces and plays a critical role in determining the reliability and performance of bonded systems, coatings, and interfaces. An appropriate understanding of this physics helps develop strategies to enhance adhesion in practical applications such as adhesives, paints, and biomedical implants (Adesanya, 2015; Khan *et al*., 2016). It also enables the design of more efficient manufacturing processes and the development of novel materials with tailored adhesive properties (Akolade *et al*., 2021; Tunc and Bayazitoglu, 2001). Shu *et al*. (2017) conducted a comprehensive review of current research on the no-slip boundary condition in fluid dynamics problems, analyzing numerical, theoretical, and experimental

* Corresponding author. Tel.: +2348169953938
E-mail address: akolade.mojeed@lcu.edu.ng (M. T. Akolade)
https://doi.org/10.62054/ijdm/0101.15

approaches and the challenges encountered therein. Limitations of applying the no-slip condition are identified in non-Newtonian fluids, such as erroneous outcomes due to the control of flow by the first principle, where slip at the boundary wall is expected. To address this issue, researchers have introduced partial slip by considering nonzero tangential components of velocity, temperature, and stress in boundary calculations. Awais *et al*. (2016) numerically investigated slip effects on viscous fluid over a stretching wall surface, identifying that the slip parameter enhanced velocity at the boundary wall while thermal-slip resulted in a reduction in temperature distribution. Tulu and Ibrahim (2021) examined the impact of second-order slip and variable viscosity on hybrid nanofluid flow through a stretching surface, concluding that incorporating second-order slip on the wall surface improved the magnitude of shear stress and conserved the rate of heat transfer.

Considerable attention is garnered due to the wide application of non-Newtonian fluids and dynamics of convection over a nonlinearly stretching surface, attributed to their significance in engineering, science, and biomedical fields. The Carreau fluid, characterized by shear thickening and thinning properties, finds application in various materials such as blood, mucus, yogurt, lotion, and shampoo. Irfan *et al*. (2021) introduced the convective aspects of thermal heat on Carreau fluid motion, while Khan *et al*. (2018) accounted for multiple solutions for Carreau fluid flow over a nonlinearly stretching surface. Nabwey *et al*. (2022) analyzed the convection flow of Carreau fluid over a cylinder while Hashim *et al*. (2020) investigated the mixed convection flow and heat transfer mechanism for non-Newtonian Carreau nanofluids under the effect of infinite shear rate viscosity. Other notable studies include, Akolade (2023) where second law analysis of a dissipative Carreau fluid dynamics over nonlinear stretching sheet was investigated, Khan *et al*. (2020) presented the stagnation point flow of non-Newtonian fluid (Carreau fluid) with Cattaneo-Christov heat flux, Khan *et al*. (2018) investigated the solutions for non-Newtonian Carreau fluid flow over an inclined shrinking sheet, Khan and Hashim (2015) explained the boundary layer flow and heat transfer to Carreau fluid over a nonlinear stretching sheet, and Anguiano *et al*. (2022) discussed Carreau law for non-Newtonian fluid flow through thin porous media.

The current studies aim at analyzing the dynamics of magnetized, non-Newtonian Carreau fluid flow over an inclined nonlinear stretching surface with quadratic thermal convection via the implementation of the Chebyshev Collocation Method (CCM) with a pseudo-spectral approach. This novel investigation of momentum, energy, and second law analysis is subjected to second-order slip and jump conditions, Joule heating, nonlinear radiation, space, and temperature-dependent heat modulations. Herein, we seek to identify the best working fluid rheology in the design domain for proper prediction, implementation, and utilisation in engineering system. Furthermore, we believe that assumptions in this investigation will enable engineers, scientists, and modellers, among others, to predict the behaviour and characteristics of the fluid rheology (shear thinning and shear thickening) and make efficient/judicious application of it.

2. Model Analysis

Figure 1 describes the two-dimensional, magnetized, incompressible and steady state heat transfer of Carreau fluid over an inclined slendering sheet subject to temperature jump and second-order velocity slip conditions for nonlinear thermal convection, radiation, and viscous dissipation Carreau fluid. The magnetic field of strength $B(x) = B_0 x^{(m-1)/2}$, with the initial stretching characteristics $U_0 = d_0 x^m$ in the axis $y = A\, x^{(1-m)/2}$.

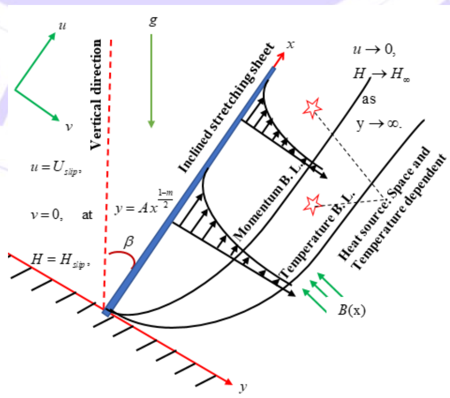

Figure 1: Physical Flow Geometry.

The Carreau constitutive model is described by (Akolade *et al*., 2022; Akolade, 2023; Hashim et al., 2017; Khan et al., 2019):

$$\tau = -PI + \mu\dot{\gamma}K_1, \mu = \mu_\infty + (\mu_0 - \mu_\infty)[1 + (\Gamma\dot{\gamma})^2]^{\frac{n-1}{2}}, \quad \text{and } \dot{\gamma} = \sqrt{\frac{1}{2}\Pi} \quad \Pi = trace(K_1^2) \tag{1}$$

Flow convection process by nonlinear Boussinesq approximation is taken to be (Akolade *et al*., 2022; Ibrahim and Gamachu, 2019; Yadav *et al*., 2024);

$$\Xi(H) = -\rho[\beta_1(H - H_\infty) + \beta_2(H - H_\infty)^2], \tag{2}$$

Following Akolade *et al*. (2022), the temperature dependent function of variable thermal conductivity and electrical conductivity is given by:

$$\kappa(H) = \kappa^* e^{(-\epsilon_0(T-T_\infty))} \approx \kappa^*[1 - \epsilon_0(H - H_\infty)], \quad \sigma^*(H) = [1 + \xi_0(H - H_\infty)]. \tag{3}$$

The heat flux Rosseland approximation is defined as:

$$q_r = -\frac{4\sigma^t}{3k_t}\frac{\partial H^4}{\partial y} = -\frac{16\sigma^t}{3k_t}(H^3\frac{\partial H}{\partial y}), \tag{4}$$

And the adherence between the flowing fluid and the solid boundaries is given by:

$$U_{slip} = \frac{\mu}{\rho}[a_1\frac{\partial u}{\partial y} - a_2\frac{\partial^2 u}{\partial y^2}], \quad H_{slip} = b_1\frac{\partial H}{\partial y} + b_2\frac{\partial^2 H}{\partial y^2}. \tag{5}$$

Subject to above stated conditions, the govering PDEs driving the Carreau fluid flow is given by (Akolade *et al*., 2022; Akolade, 2023; Hashim *et al*., 2017; Khan *et al*. 2019):

$$\frac{\partial u}{\partial x} + \frac{\partial v}{\partial y} = 0, \tag{6}$$

$$\left\{\left[1 + \Gamma^2\left(\frac{\partial u}{\partial y}\right)^2\right]^{\frac{n-1}{2}} + (n-1)\Gamma^2\left[1 + \Gamma^2\left(\frac{\partial u}{\partial y}\right)^2\right]^{\frac{n-3}{2}}\left(\frac{\partial u}{\partial y}\right)^2\right\}\nu\frac{\partial^2 u}{\partial y^2} = u\frac{\partial u}{\partial x} + v\frac{\partial u}{\partial y} + \frac{\sigma^*(H)B(x)^2}{\rho}u + g\cos(\beta)\frac{\Xi(H)}{\rho}, \tag{7}$$

$$\begin{aligned} u\frac{\partial H}{\partial x} + v\frac{\partial H}{\partial y} - \frac{1}{\rho C_p}\frac{\partial}{\partial y}\left(\kappa(H)\frac{\partial H}{\partial y}\right) &= \frac{1}{\rho c_p}\frac{k^* U_0}{x\nu}[B_1 e^{-\eta}(H_w - H_\infty) + B_2(H - H_\infty)] - \frac{1}{\rho c_p}\frac{\partial q_r}{\partial y} \\ &+ \frac{\sigma^*(H)B(x)^2}{\rho C_p}u^2 + \frac{\mu}{\rho C_p}\left\{\left[1 + \Gamma^2\left(\frac{\partial u}{\partial y}\right)^2\right]^{\frac{n-1}{2}} + (n-1)\Gamma^2\left[1 + \Gamma^2\left(\frac{\partial u}{\partial y}\right)^2\right]^{\frac{n-3}{2}}\left(\frac{\partial u}{\partial y}\right)^2\right\}\left(\frac{\partial u}{\partial y}\right)^2. \end{aligned} \tag{8}$$

Subject to the conditions:

$$u = U_w(x) + U_{slip}, \quad v = 0, H = H_w + H_{slip}, \quad at \ \ y = Ax^{\frac{1-m}{2}}, \quad u = 0, \ H = H_\infty \ \ as \ \ y \to \infty. \tag{9}$$

Adopting the similarity variables from the recent studies of (Akolade *et al*., 2022; Akolade, 2023; Hashim *et al*., 2017; Khan *et al*., 2019);

$$u = \frac{\partial\psi}{\partial y}, \quad v = -\frac{\partial\psi}{\partial x}, \quad \psi = \left(\frac{2\nu d_0 x^{m+1}}{m+1}\right)^{\frac{1}{2}} f(\eta), \quad \theta(\eta) = \frac{H - H_\infty}{H_w - H_\infty}, \ \eta = \left(\frac{(m+1)d_0 x^{m-1}}{2\nu}\right)^{\frac{1}{2}} y. \tag{10}$$

Then, applying equation (10) on Eqns. (7) - (9), we have the reduced ordinary differential equations (ODEs):

$$\begin{gathered} \{1 + D \ We^2(f'')^2\}^{\frac{n-3}{2}}[1 + nWe^2 \ D \ (f'')^2]f''' + ff'' - \\ \frac{1}{D}[m(f')^2 + Ha^2 \ (1 + \xi_2\theta)f' - \cos(\beta)G_r(\theta + \xi_1\theta^2)] = 0, \end{gathered} \tag{11}$$

$$\begin{gathered} PrEc\{1 + D \ We^2(f'')^2\}^{\frac{n-3}{2}}[1 + nD \ We^2 \ (f'')^2](f'')^2 + Pr \ f \ \theta' + \frac{1}{D}\left[B_1 \ e^{(-\eta)} + B_2 \ \theta\right] + \\ \frac{4R_L}{3}\{(1 + (R_N - 1)\theta)^3\theta'\} + Ec \ Pr \ Ha^2 \ \frac{1}{D} \ (1 + \xi_2 \ \theta) \ (f')^2 + (1 - \xi_3\theta)\theta'' - \xi_3(\theta')^2 = 0, \end{gathered} \tag{12}$$

subjected to:

$$\begin{gathered} f'(\eta) = 1 + \Lambda_1 f''(\eta) - \Lambda_2 f'''(\eta), \quad \theta(\eta) = 1 + \Lambda_3\theta'(\eta) + \\ \Lambda_4\theta''(\eta), \quad f(\eta) = \left(\frac{1-m}{1+m}\right)\chi[f'(\eta)], \quad at \quad \eta = \chi, \\ f'(\eta) = 0, \ \ \theta(\eta) = 0, \ \ as \quad \eta \to \infty, \end{gathered} \tag{13}$$

where $D = \left(\frac{m+1}{2}\right)$, $\chi = A\sqrt{\frac{m+1}{2\nu}d_0}$, $\Lambda_1 = \frac{S_1}{\sqrt{Re_x^{-1}}}$, $\Lambda_2 = \frac{S_2}{Re_x^{-1}}$, $\Lambda_3 = \frac{S_3}{\sqrt{Re_x^{-1}}}$, $\Lambda_4 = \frac{S_4}{Re_x^{-1}}$, $Gr = \frac{\epsilon_1}{Re_x}$, $S_1 = a_1\nu\left(\frac{(m+1)}{2}\right)^{\frac{1}{2}}$, $S_2 = a_2\nu\left(\frac{(m+1)}{2}\right)$, $S_3 = b_1\nu\left(\frac{(m+1)}{2}\right)^{\frac{1}{2}}$, $S_4 = b_2\nu\left(\frac{(m+1)}{2}\right)$, $\epsilon_1 = \frac{\beta_1 g(T_w - T_\infty)}{d_0\nu U_0}$, $\xi_1 = \frac{\beta_2}{\beta_1}(T_w - T_\infty)$, $Pr = \frac{\mu Cp}{k^*}$, $We^2 = \frac{\Gamma^2 d_0^3 x^{3m-1}}{\nu}$, $R_L = \frac{4\sigma^t H_\infty^3}{k_t k^*}$, $Pr = \frac{c_p\mu}{k^*}$, $R_N = \frac{H_w}{H_\infty}$, $\xi_2 = \xi_0(H_w - H_\infty)$, $\xi_3 = \epsilon_0(H_w - H_\infty)$, $Ec =$

$\frac{U_0^2}{Cp(H_w-H_\infty)}$, $Ha = B_0\left(\frac{\sigma}{\rho d_0}\right)^{\frac{1}{2}}$, and $Re_x = \frac{U_0}{\nu x}$.
Equations (11) - (13) are then transformed to the following sets of equations using $F(\omega) = F(\eta-\chi) = f(\eta)$, and $\Theta(\omega) = \Theta(\eta-\chi) = \theta(\eta)$:

$$\{1 + D\ We^2(F'')^2\}^{\frac{n-3}{2}}[1 + nWe^2\ D\ (F'')^2]F''' + FF'' \\ -\frac{1}{D}[m(F')^2 + Ha^2\ (1+\xi_2\Theta)F' - \cos(\beta)G_r(\Theta + \xi_1\Theta^2)] = 0, \tag{14}$$

$$Pr\ Ec\ \{1 + D\ We^2(F'')^2\}^{\frac{n-3}{2}}[1 + nD\ We^2\ (F'')^2](F'')^2 + Ec\ Pr\ Ha^2\ \frac{1}{D}(1+\xi_2\ \Theta)(F')^2 + \\ Pr\ F\ \Theta' + \frac{1}{D}\left[B_1\, e^{(-\omega)} + B_2\,\Theta\right] + \frac{4R_L}{3}\{(1 + (R_N-1)\Theta)^3\Theta'\} + (1-\xi_3\Theta)\Theta'' - \xi_3(\Theta')^2 = 0, \tag{15}$$

subjected to:

$$F'(\omega) = 1 + \Lambda_1 F''(\omega) - \Lambda_2 F'''(\omega), \quad \Theta(\omega) = 1 + \Lambda_3\Theta'(\omega) + \Lambda_4\Theta''(\omega), \\ F(\omega) = \left(\frac{1-m}{1+m}\right)\chi\, F'(\omega), \quad at\ \ \omega = 0, \quad F'(\omega) = 0,\ \Theta(\omega) = 0,\ as\ \ \omega\to\infty. \tag{16}$$

Also, the physical quantities are defined accordinly:

$$Re_x^{\frac{1}{2}}C_{f_x} = \sqrt{\frac{m+1}{2}}F''(0)[1 + We^2\ (F''(0))^2]^{\frac{n-1}{2}}, \\ Re_x^{-\frac{1}{2}}Nu_x = -(1 - \xi_3\Theta(0) + \frac{4}{3}R_L(1 + (R_N-1)\Theta(0))^3)\Theta'(0). \tag{17}$$

2.1 Second law analysis

The corresponding second law equations are derived accordinly:

$$Entropygeneration\ (E_G) = HeatTransferIrreversibility + FluidFrictionIrreversibility. \tag{18}$$

Heat Transfer Irreversibility (HTI)

$$\text{HTI} = \frac{1}{H_\infty^2}\left\{\kappa(H) + \frac{16\sigma^t}{3k_t}H^3\right\}\left(\frac{\partial H}{\partial y}\right)^2. \tag{19}$$

Fluid Friction Irreversibility (FFI)

$$\text{FFI} = \left\{\left[1 + \Gamma^2\left(\frac{\partial u}{\partial y}\right)^2\right]^{\frac{n-1}{2}} + (n-1)\Gamma^2\left[1 + \Gamma^2\left(\frac{\partial u}{\partial y}\right)^2\right]^{\frac{n-3}{2}}\left(\frac{\partial u}{\partial y}\right)^2\right\}\frac{\mu}{H_\infty}\left(\frac{\partial u}{\partial y}\right)^2 + \frac{\sigma^*(H)}{H_\infty}B(x)^2u^2. \tag{20}$$

Implementing the similarity variables in Eq. (10) on the dimensional second law system of Eq. (18), gives:

$$Ns = \frac{E_G}{E_{G_0}'''} = D\ \left[1 - \xi_3\Theta + \frac{4R_L}{3}(1 + (R_N-1)\Theta)^3\right](\Theta')^2 + Pr\ Ec\ L\ Ha\ (1+\xi_2\ \Theta)(F')^2 + \\ Pr\ Ec\ L\ D\ \{1 + D\ We^2(F'')^2\}^{\frac{n-3}{2}}[1 + nD\ We^2\ (F'')^2](F'')^2. \tag{21}$$

where E_{G_0}''', L are defined below.

$$E_{G_0}''' = \frac{\kappa^*}{\nu}\frac{(H_w-H_\infty)^2\ d_0^3}{H_\infty^2\ U_0^2}, \quad L = \frac{H_\infty}{H_w-H_\infty}. \tag{22}$$

Moreover, Bejan number is defined as the ratio of ***HTI*** to Ns i.e.,

$$Be = \frac{HTI}{HTI+FFI} = \frac{HTI}{Ns}. \tag{23}$$

3. Method of Solution

Solutions of the coupled equations (14) - (16) is obtained by adopting the Chebyshev differention matrix based collocation method. The techniqe enjoy the algebraic mapping transformation of the problem physical domain into the Chebysev domain $\tau \in [-1,1]$:

$$\tau = \frac{2\omega}{L} - 1, \qquad \tau \in [-1,1]. \tag{24}$$

Also, an assumption of the trial solution for $F(\tau)$, and $\Theta(\tau)$ is given by;

$$F(\tau) \approx F_N(\tau) = \sum_{i=0}^{N} F(\tau_i)\xi_i(\tau), \dots,\ \ \Theta(\tau) \approx \Theta_N(\tau) = \sum_{i=0}^{N}\Theta(\tau_i)\xi_i(\tau), \dots, \tag{25}$$

with Lobbatto collocation point,

$$\tau_i = \cos\left(\frac{i\pi}{N}\right), \qquad i = 0,1,2\cdots N \tag{26}$$

and $\xi_i(\tau)$ denote the Lagrange interpolation polynomial corresponding to the Chebysev polynomial of order N,

$$T_N(\tau) = \cos(N\cos^{-1}\tau). \tag{27}$$

The Chebyshev differentiation matrix D of size $(N+1)\times(N+1)$ is adopted.
The derivative series of profile $f_n(\tau)$, $\Theta_n(\tau)$ at $\tau=\tau_i$ is given by:

$$\frac{dF(\tau_i)}{d\tau}=\sum_{j=0}^{N} D_{i,j}^{(1)}F(\tau_j),\quad \frac{dF^n(\tau_i)}{d\tau^n}=\sum_{j=0}^{N} D_{i,j}^{(n)}F(\tau_j),$$
$$\frac{d\Theta(\tau_i)}{d\tau}=\sum_{j=0}^{N} D_{i,j}^{(1)}\Theta(\tau_j),\quad \frac{d\Theta^n(\tau_i)}{d\tau^n}=\sum_{j=0}^{N} D_{i,j}^{(n)}\Theta(\tau_j), \tag{28}$$

where $i=0,1,\cdots N$. Substituting equation (28) into the dimensionless governing Eqs. (14) - (16), then solve via Newton's method, the unknown functions $F(\tau_i)$, and $\Theta(\tau_i)$ containing $2N+2$ equations with $2N+2$ unknowns variables are derived. Finally, the result obtained is now in domain $\tau\in[-1,1]$ which is then transformed into $\omega\in[0,L]$using;

$$\eta=\frac{L}{2}(\tau+1),\qquad \tau\in[0,L]. \tag{29}$$

Table 1: Comparison results of $F''(0)$ and $-\Theta'(0)$ with eariler studies at different Λ_1 χ andPr.

Value		$-F''(0)$		Value	$-\Theta'(0)$ such that $\Lambda_1=\chi=0$		
Λ_1	χ	Devi and Prakash (2016)	Present work	Pr	Mabood *et al.* (2015)	Sharma *et al.* (2022)	Present work
0.0	0.2	0.9248281	0.924821298	0.2	0.1691	0.16631332	0.17003133
0.2	0.25	0.7333949	0.733385610	0.7	0.4539	0.45540012	0.45391747
0.2	0.3	–	0.738594316	2.0	0.9114	0.91102381	0.91135768
0.2	0.5	0.7595701	0.759562561	7.0	1.8954	1.89432002	1.89431426
0.5	0.5	–	0.578436131	20	3.3539	3.35045413	3.35065976
0.5	0.6	–	0.584199971	70	6.4622	6.46010020	6.46011132

4. Results and Discussion

Impact of the controling parameters on the dimensionless distribitions is enumerated in this section. Reference to the previous studies, the following choice of the parameters are adopted else otherwise stated ($\chi=0.5, m=1/3$, $n=0.2$, $Pr=7.2$, $We=5$, $B_1=0.07=B_2$, $Ha=1$, $Gr=1$, $\xi_1=1$, $\xi_2=0.2$, $\xi_3=0.5$, $\beta=\pi/3$, $\Gamma_2=0.5$, $\Gamma_4=0.2$, $\Gamma_1=0.2$, $\Gamma_3=0.2$, $R_N=1.3$, $R_L=0.3$, $Ec=0.1$). In Table 1, accuracy and workability of the spectral collocation method adopted for this study is demostrated with the previous studies of Devi and Prakash (2016), Mabood *et al*. (2015), and Sharma *et al*. (2022). It is worth mentioning that the limited case of our model tally with the previous studies.

Analysis of flow distribution enumerating the impact of supporting model variables is identified in the respective Figures 2-7, both on the momentum, energy Bejan number and irriversibility distribution ratio. As pictured in Figure 2 and 3, the fluid rheological characterization (n) providing insight into the dynamics of Carreau fluid is identified (shear-thickening fluid $(n>1)$, shear-thinning fluid $(n<1)$). Moreover, analysis into the dynamics of different heat source module is presented. A closer look on Figures 2(b), and 3(b) identified that the temperature dependent heat source module is capable of decomposing the fluid particles in sorter time compare to the space-dependent heat sourec module. However, the two modles display a rise to both velocity and temperature of the fluid. The report of the fluid characterization $(n>1)$ and $(n<1)$ show that shear-thinning fluid conduct heat energy easily compare to the shear-thickening fluid, thereby loose it particles easily. However, a deflection point $\omega\approx 2$, is identified as phase change between the shear-thinning fluid and the shear-thickening fluid. For the boundary layer length $\omega<2$, the shear-thickening fluid demostrated a higher momentum rate while shear-thinning fluid showcase its higher momentum rate just after the deflection piont $\omega>2$. In general, this analysis help predict the right rehological model for the purpose of industrial proces.

Assesment of the inclination angle (β) and the Hartmann number (Ha) on momentum field and thermal field is depicted in Figure 4(a and b). While Ha shows its ability to decline the momentum field, the contrary response is percived on the energy distribution. Inline with the physiscs of the Lorentz force, intesification of the magnetization effect draged down the motion of the fluid thereby enhancing the fluid thermal performance. At the same time, the energy distribution is upsurgeed as both Ha and β are elevated. The imposed inclined angle as well shows its ability to drag down the strength of Lorentz's force. Relation between the enthalpy of the boundary layer and momentum kinetic energy, known as Eckert number and the adherence factors (first and second-order slip/jump) is enumerated in Figure 5(a and b). The profiles clarified that as heat dissipated increases (rise in Ec) the flow field and energy distribution upsurge. Hoever, magnification is more pronouced in the fluid temperature for no adherence (slip and jump) condition than the presence of slip and jump instance.

Convection analysis of nonlinear/linear thermal (ξ_1,Gr) over profiles of velocity and energy is identified in Figure 6(a and b). The opposing force due to the acceleration due to gravity, Physically, upright impact of flow geometry predicts the higher impact of acceleration due to gravity, while an inclined geometry tends to produce less impact of gravity. Mathematically, $\xi_1 = 0$ represent a no convection model, $\xi_1 \neq 0$ represent a nonlinear convection model. From the analysis, a rise in convection term signifies a raise in momentum field, and a reduction in energy distribution. For practical use, a nonlinear model is suggest for more interference on both temperature and velocity than the linear assumption (see Figure 6a and 6b). The interaction of the variable thermal conductivity (ξ_3) and electrical conductivity (ξ_2) is illuminated in Figure 7. Mathematically, $\xi_2 = 0$ reduced the model to a constant electrical field. Like the impact of Ha, ξ_2 also drags down the momentum and elevates the energy field due to Lorentz force activation. On the other hand, variable thermal conductivity (ξ_3) diminished the Carreau fluid momentum and energy field considerably. This result itemized that grater numbers of ξ_3 reduced the conductivity of Carreau fluid.

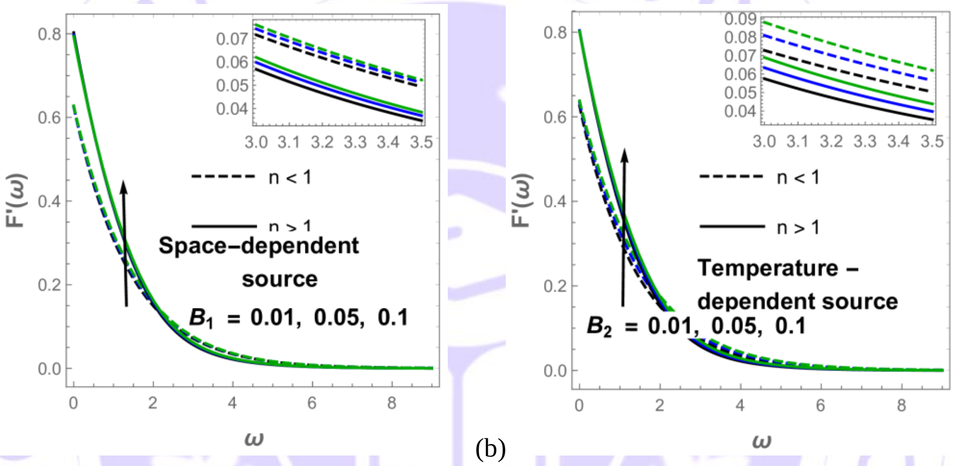

(a) (b)

Figure 2: Profiles $F'(\omega)$ for different B_1, B_2 and n.

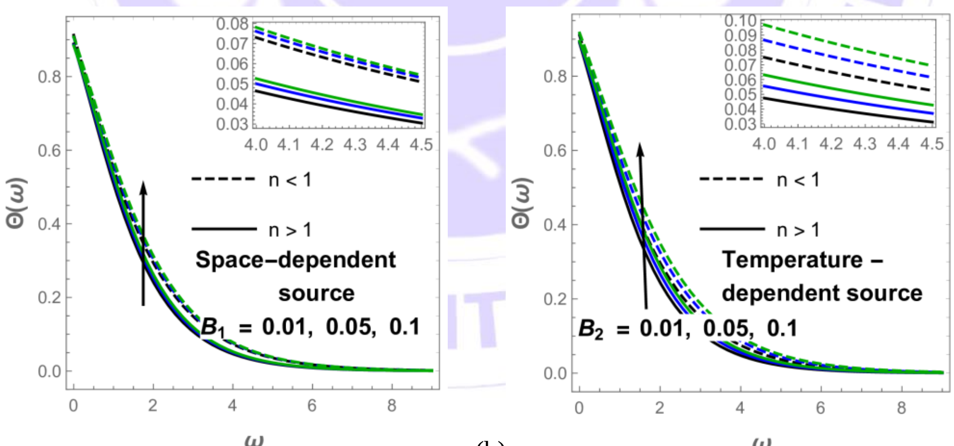

(a) (b)

Figure 3: Profiles $\Theta(\omega)$ for different B_1, B_2 and n.

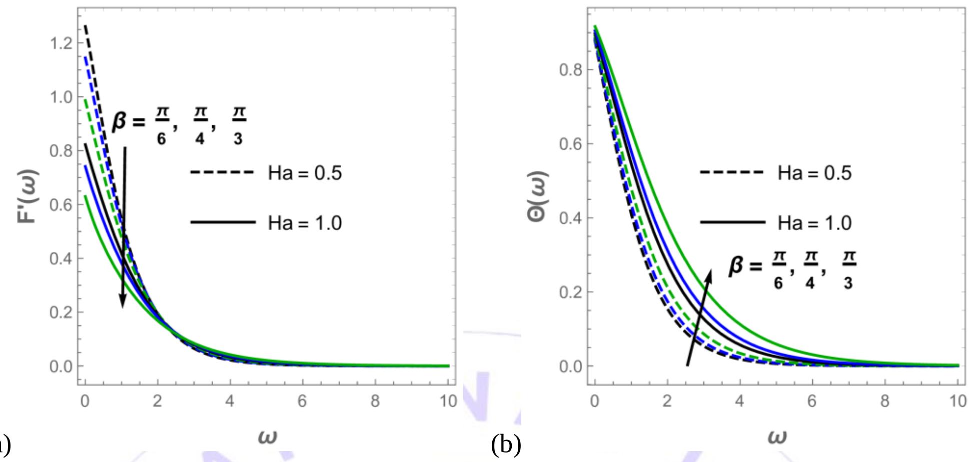

Figure 4: Profiles $F'(\omega)$ and $\Theta(\omega)$ for different β and Ha.

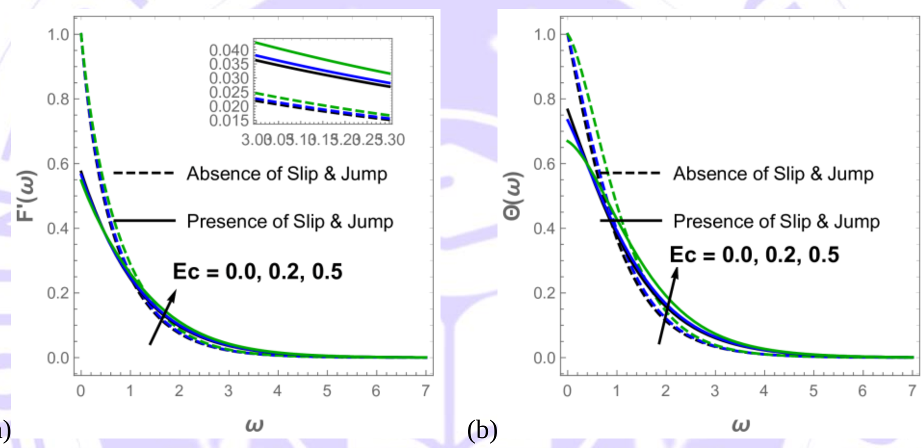

Figure 5: Profiles $F'(\omega)$ and $\Theta(\omega)$ for different Ec and slip/jump conditions.

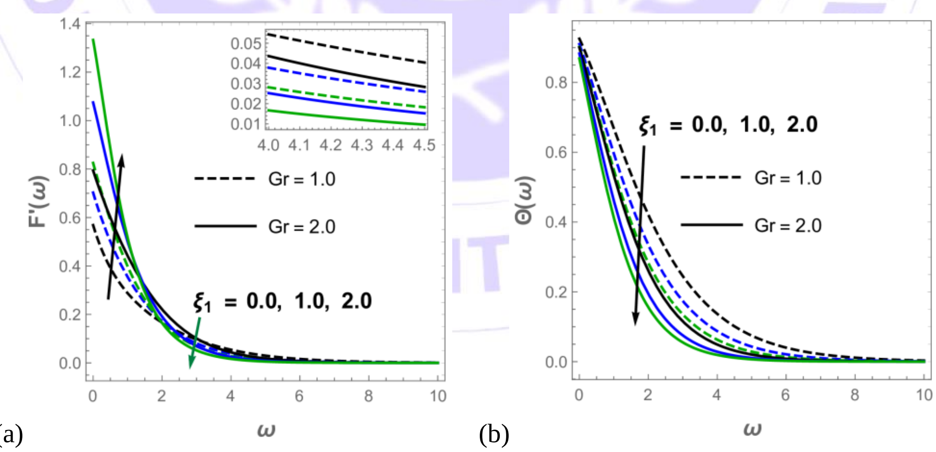

Figure 6: Profiles $F'(\omega)$ and $\Theta(\omega)$ for different Gr and ξ_1.

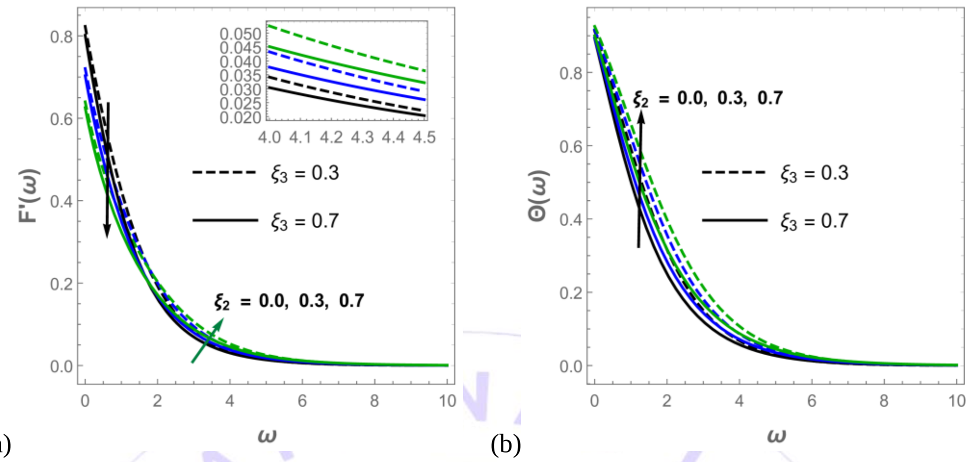

(a) (b)

Figure 7: Profiles $F'(\omega)$ and $\Theta(\omega)$ for different ξ_2 and ξ_3.

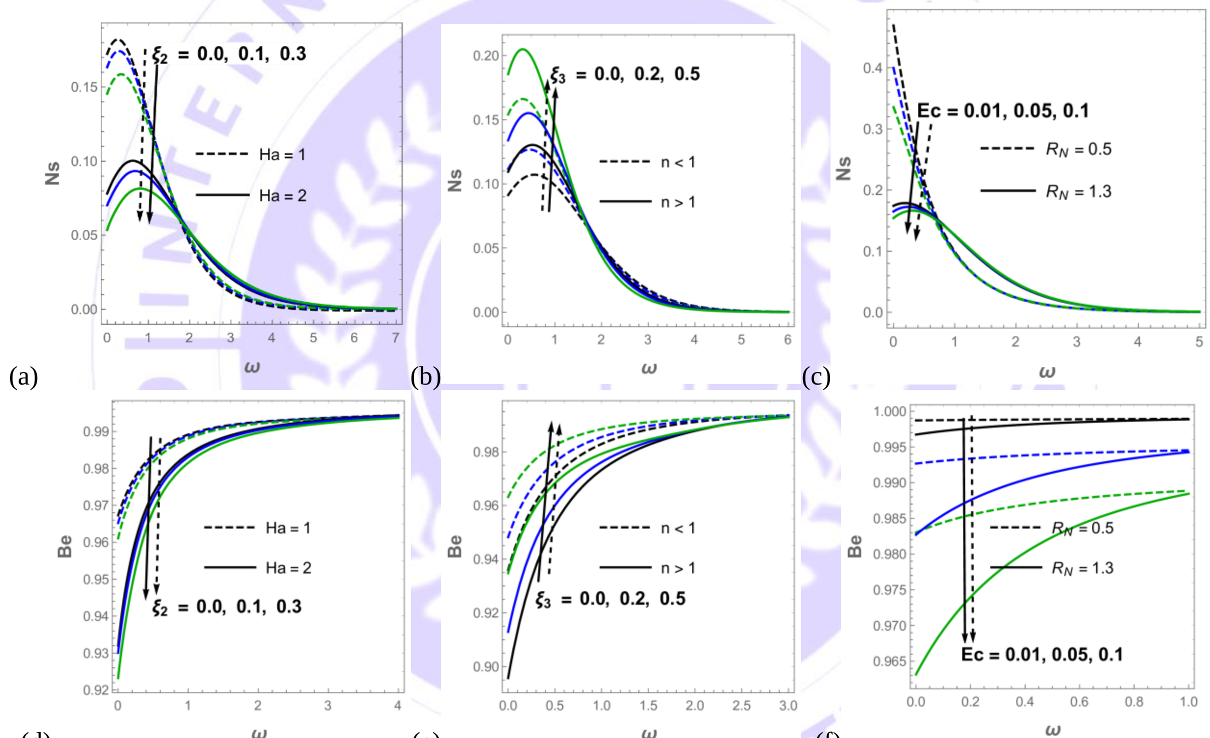

(a) (b) (c)

(d) (e) (f)

Figure 8: Profile Ns for differentR_N, Ec, n, ξ_3, ξ_2 and Ha,,, Profile Be for different R_N, Ec, n, ξ_3, ξ_2 and Ha

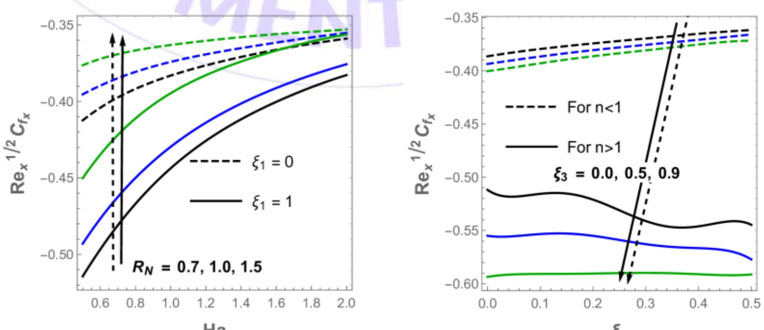

(a) (b)

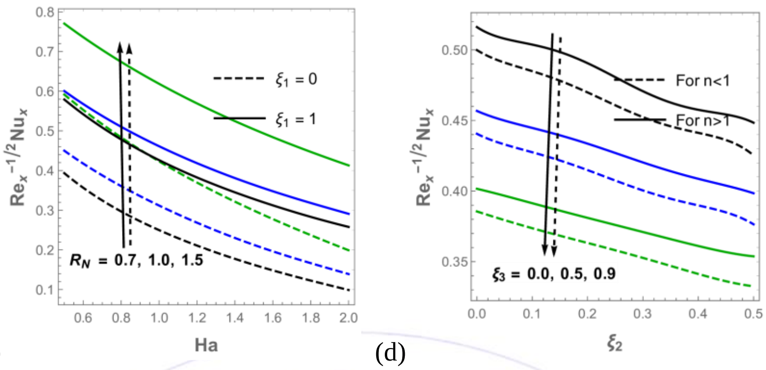

(c) (d)

Figure 9: Profiles of $Re_x^{\frac{1}{2}}C_{f_x}$ and $Re_x^{-\frac{1}{2}}Nu_x$ for different R_N, n, ξ_3, ξ_2 and Ha

To identify the dominance of entropy generation and irreversibility process in thermal to fluid friction in the considered flow configuration, Figure 8(a-f) enumerated the characterized behaviour of the flow parameters (Ha, ξ_2, ξ_3, n, Ec, and R_N) on Ns and Be accordingly. Mathematically, $Be > 0.5$ represent the dominance of thermal irreversibility, $Be = 0.5$ highlights the equal contribution of thermal to fluid friction irreversibility, and $Be < 0.5$ enumerated the irriversibility due to fluid friction. Introduction of magnetization effect optimized the entropy generation (Ns) and irreversibility distribution ratio (Be) for both constant (Ha) and variable (ξ_2) assumption. Shear-thinning fluid demonstrated the ability to produce higher entropy generation in contrast to the Shear thickening fluid as shown in Figure 8(b), while the contrary result is produced on Bejan number as profiled on Figure 8(e). A rise in R_N as depicted in Figure 8(c) injected more heat into the system, thus optimizing (reducing) the entropy production. Mathematically, R_L radiative heat flux is an approximated form of R_N; the exact impact is felt as radiative heat fluxes rise. Furthermore, as seen in Figure 8(f), frictional heating irreversibility is dominated by heat transfer irreversibility with an increasing value of R_N. Similarly, the contribution of the frictional forces Ec (i.e. the relation between the enthalpy variance and fluid temperature) shrinks Ns and Be, indicating that higher Ec and R_N is a contributing parameter to reduced system disorderliness. Moreover, thermal irreversibility is seen dominating the entire flow system. Higher dominance is recorded at the far free stream of the considered geometry (see Fig. 8).

The computational results of the Local skin friction and heat transfer coefficients depicted in Figure 9(a-d) highlighted the tendency of the two physical properties to diminish based on fluid classification (n) from shear-thickening fluid to shear-thinning fluid. This enumerates that more flow strength is induced in shear-thickening fluid compared to others (shear-thinning and Newtonian fluid). A rise in the inclination angle (β) correspond to magnification of both local $Re_x^{1/2}C_{f_x}$ and $Re_x^{-1/2}Nu_x$. However, variability of thermal conductivity (ξ_3) energized the heat transfer coefficient and contributed to the minimization of the skin friction coefficient.

5. Conclusion

The Carreau fluid rheology classified as shear-thinning ($n < 1$), shear-thickening ($n > 1$) and Newtonian ($n = 1$) fluids has been investigated. The considered nonlinear stretching model proposed the higher adherence jump, slip, space and temperature-dependent heat modules. Nonlinear radiation heat flux, joule heating, nonlinear convection, and variable thermal conductivity is considered. Subjected to the similarity variables, the transformed ODE systems of the inclined suspended motion over a thin sheet pictured in Figure 1 employed a Spectral collocation scheme to carry out the approximate solution of the distribution profiles ($F'(\omega)$, $\Theta(\omega)$, $Ns(\omega)$ and $Be(\omega)$). The findings highlight that:

1. more heat is dissipated as Ec grows and Joule heating effect generate inner energy which induced the Carreau fluid energy;
2. nonlinear convection model predicts more interference on both momentum and energy contrast to the linear model;
3. the results elucidate the tendency of both heat source modulation to minimize heat transfer coefficient;
4. local skin-friction and Nusselt number diminished based on fluid classification (n) from shear-thickening fluid to shear-thinning fluid;
5. variability of thermal conductivity (ξ_3) energized the heat transfer coefficient and contributed to minimizing the skin friction coefficient;

6. thermal irreversibility dominated the entire flow system;
7. dissipative function, radiation heat flux, and magneto-hydrodynamic modules are identified mechanisms for minimizing both entropy generation and Bejan number;
8. for further entropy generation and Bejan number promotion, more thermal enhancement is required.

Conflict of Interest

The authors have declared no conflict of interest.

References

Adesanya, S. O. (2015). Free convective flow of heat generating fluid through a porous vertical channel with velocity slip and temperature jump. *Ain Shams Engineering Journal*, 6(3), 1045-1052. https://doi.org/10.1016/j.asej.2014.12.008

Akolade, M. T. (2023). Numerical approach to second law analysis of a dissipative Carreau fluid dynamics over nonlinear stretching sheet. *International Journal of Ambient Energy*, 44(1), 1427-1437. https://doi.org/10.1080/01430750.2023.2175725

Akolade, M. T., Agunbiade S. A., and Oyekunle T. L. (2022). Onset modules of heat source and generalized Fourier's law on Carreau fluid flow over an inclined nonlinear stretching sheet, *International journal of modelling and simulation*. DOI: 10.1080/02286203.2022.2151964

Akolade, M. T., Idowu, A. S., and Adeosun, A. T. (2021). Multi-slip and Soret-Dufour influence on nonlinear convection flow of MHD dissipative Casson fluid over a slendering stretching sheet with generalized heat flux phenomenon. *Heat Transfer*. 2021;1-21. https://doi.org/10.1002/htj.22057

Anguiano, M., Bonnivard, M., and Suárez-Grau, F. J. (2022). Carreau law for non-Newtonian fluid flow through a thin porous media. *The Quarterly Journal of Mechanics and Applied Mathematics*, 75(1), 1-27. https://doi.org/10.1093/qjmam/hbac004

Awais M., Hayat T., Ali A., and Irum S. (2016). Velocity, thermal and concentration slip effects on a magnetohydrodynamic nanofluid flow. *Alexandria Engineering Journal*. 55, 2107-2114. https://doi.org/10.1016/j.aej.2016.06.027

Bejan, A. (1995). Entropy Generation Minimization: The Method of Thermodynamic Optimization of Finite-Size Systems and Finite-Time Processes (1st ed.). *CRC Press*. https://doi.org/10.1201/9781482239171

Bejan, A. (1996). Entropy generation minimization: The new thermodynamics of finite-size devices and finite-time processes. *Journal of Applied Physics*, 79(3), 1191-1218. https://doi.org/10.1002/9781119245964.ch11

Bejan, A. (2002). Fundamentals of exergy analysis, entropy generation minimization, and the generation of flow architecture. *International journal of energy research*, 26(7). https://doi.org/10.1002/er.804

Devi, S. P. A., and Prakash, M. (2016). Slip Flow Effects over Hydromagnetic Forced Convective Flow over a Slendering Stretching Sheet, *Journal of Applied Fluid Mechanics*, Vol. 9, No. 2, pp. 683-692.

Hashim, M. Khan, A.S., and Alshomrani, D. A. (2017). Numerical simulation for flow and heat transfer to Carreau fluid with magnetic field effect: Dual nature study, *Journal of Magnetism and Magnetic Materials* (2017), doi: http://dx.doi.org/10.1016/j.jmmm.2017.06.135

Hashim, M., Sardar, H., and Khan M. (2020). Mixed convection flow and heat transfer mechanism for non-Newtonian Carreau nanofluids under the effect of infinite shear rate viscosity. *Physica Scripta*. 2020, 95(3), 035225. 10.1088/1402-4896/ab41e9

Ibrahim, W., and Gamachu, D. (2019). Nonlinear convection flow of Williamson nanofluid past a radially stretching surface. *AIP Advances*, 9(8). doi: 10.1063/1.5113688

Irfan, M., Rafiq, K., and Anwar, M.S. (2021) Evaluating the performance of new mass flux theory on Carreau nanofluid using the thermal aspects of convective heat transport. *Pramana J. Phys*. 95, 203. https://doi.org/10.1007/s12043-021-02217-7

Khan, A., Sohail, A., Rashid, S., Rashidi, M. M., and Alam Khan, N. (2016). Effects of slip condition, variable viscosity and inclined magnetic field on the peristaltic motion of a non-Newtonian fluid in an inclined asymmetric channel. *Journal of Applied Fluid Mechanics*, 9(3), 1381-1393. 10.18869/ACADPUB.JAFM.68.228.24417

Khan, M. I., Kumar, A., Hayat, T., Waqas, M., and Singh, R. (2019). Entropy generation in flow of Carreau nanofluid. *Journal of Molecular Liquids.* 278, 677-687. https://doi.org/10.1016/j.molliq.2018.12.109

Khan, M. I., Nigar, M., Hayat, T., and Alsaedi, A. (2020). On the numerical simulation of stagnation point flow of non-Newtonian fluid (Carreau fluid) with Cattaneo-Christov heat flux. *Computer Methods and Programs in Biomedicine*, 187, 105221. https://doi.org/10.1016/j.cmpb.2019.105221

Khan, M., and Hashim, H. (2015). Boundary layer flow and heat transfer to Carreau fluid over a nonlinear stretching sheet. *AIP Advances*, 5(10). https://doi.org/10.1063/1.4932627

Khan, M., Sardar, H., Gulzar, M. M., and Alshomrani, A. S. (2018). On multiple solutions of non-Newtonian Carreau fluid flow over an inclined shrinking sheet. *Results in physics*, 8, 926-932. https://doi.org/10.1016/j.rinp.2018.01.021

Khan, M., Sardar, H., Gulzar, M. M., and Alshomrani, A.S. (2018). On multiple solutions of non-Newtonian Carreau fluid flow over an inclined shrinking sheet, *Results in Physics*. doi: https://doi.org/ 10.1016/j.rinp.2018.01.021

Lone, S. A., Khan, A., Gul, T., Mukhtar, S., Alghamdi, W., and Ali, I. (2024). Entropy generation for stagnation point dissipative hybrid nanofluid flow on a Riga plate with the influence of nonlinear convection using neural network approach. *Colloid and Polymer Science*, 1-26. https://doi.org/10.1007/s00396-024-05227-0

Mabood, F., Khan, W.A., and Ismail, I.A.M. (2015). MHD boundary layer flow and heat transfer of nanofluids over a nonlinearly stretching sheet: a numerical study, *Journal of Magnetism and Magnetic Materials*, 374, 659-576. https://doi.org/10.1016/j.jmmm.2014.09.013

Motsa, S. S., Dlamini, P., and Khumalo, M. (2014). Spectral Relaxation Method and Spectral Quasilinearization Method for Solving Unsteady Boundary Layer Flow Problems. *Advances in Mathematical Physics*, 1-12. https://doi.org/10.1155/2014/341964

Ogunsola, A. W., and Oyedotun, M. F. (2023). Effects of nonlinear thermal radiation on magnetized Al2O3-Blood nanofluid flow through an inclined microporous channel: An investigation of second law analysis. *Electrophoresis*. https://doi.org/10.1002/elps.202300157

Rashidi, M. M., Akolade, M. T., Awad, M. M., Ajibade, A. O., and Rashidi, I. (2021). Second law analysis of magnetized Casson nanofluid flow in squeezing geometry with porous medium and thermophysical influence. *Journal of Taibah University for Science*, 15(1), 1013-1026. https://doi.org/10.1080/16583655.2021.2014691

Raza, R., Mabood, F., and Naz, R. (2020). Entropy analysis of non-linear radiative flow of Carreau liquid over curved stretching sheet. *International Communications in Heat and Mass Transfer*, 119, 104975. https://doi.org/10.1016/j.icheatmasstransfer.2020.104975

Reedy, S., Srihari, P., Ali, F., and Naikoti, K. (2022). Numerical analysis of Carreau fluid flow over a vertical porous microchannel with entropy generation. *Partial Differential Equations in Applied Mathematics*, 5, 100304.

https://doi.org/10.1016/j.padiff.2022.100304

Sciacovelli, A., Verda, V., and Sciubba, E. (2015). Entropy generation analysis as a design tool—A review. *Renewable and Sustainable Energy Reviews*, 43, 1167-1181. https://doi.org/10.1016/j.rser.2014.11.104

Sharma R.P., and Shaw S. (2022). MHD Non-Newtonian Fluid Flow past a Stretching Sheet under the Influence of Non-linear Radiation and Viscous Dissipation, *J. Appl. Comput*. Mech., 8(3), 949-961. 10.22055/JACM.2021.34993.2533

Shashikumar, N. S., Sindhu, S., Madhu, M., and Gireesha, B. J. (2022). Second law analysis of MHD Carreau fluid flow through a microchannel with thermal radiation. *Waves in Random and Complex Media*, 1-25. https://doi.org/10.1080/17455030.2022.2060532

Shehzad, S. A., Madhu, M., Shashikumar, N. S., Gireesha, B. J., and Mahanthesh, B. (2021). Thermal and entropy generation of non-Newtonian magneto-Carreau fluid flow in microchannel. *Journal of Thermal Analysis and Calorimetry*, 143, 2717-2727. https://doi.org/10.1007/s10973-020-09706-8

Shu, J. J., Bin Melvin Teo, J., and Kong Chan, W. (2017). Fluid velocity slip and temperature jump at a solid surface. *Applied Mechanics Reviews*, 69(2), 020801. https://doi.org/10.1115/1.4036191

Trefethen, L. N. (2000). Spectral Methods in MATLAB, Society for Industrial and Applied Mathematics, https://epubs.siam.org/doi/abs/10.1137/1.9780898719598

Tulu, A., and Ibrahim, W. (2021). Effects of Second-Order Slip Flow and Variable Viscosity on Natural Convection Flow of CNTs-Fe_3O_4/Water Hybrid Nanofluids due to Stretching Surface. *Mathematical Problems in Engineering*, 1-18. https://doi.org/10.1155/2021/8407194

Tunc, G., and Bayazitoglu, Y. (2001). Heat transfer in microtubes with viscous dissipation. *International Journal of Heat and Mass Transfer*, 44(13), 2395-2403. https://doi.org/10.1016/S0017-9310(00)00298-2

Yadav, D., Nair, S. B., Awasthi, M. K., Ragoju, R., and Bhattacharyya, K. (2024). Linear and nonlinear investigations of the impact of chemical reaction on the thermohaline convection in a permeable layer saturated with Casson fluid. *Physics of Fluids*, 36(1). https://doi.org/10.1063/5.0187286

Zhang, Q., Tang, A., Cai, T., and Huang, Q. (2024). Analysis of entropy generation and exergy efficiency of the methane/dimethyl ether/air premixed combustion in a micro-channel. *International Journal of Heat and Mass Transfer*, 218, 124801. https://doi.org/10.1016/j.ijheatmasstransfer.2023.124801